Surface-consistent matching filters for time-lapse seismic processing

Mahdi Almutlaq and Gary F. Margrave

ABSTRACT

We introduce the concept of surface-consistent matching filters for processing time-lapse seismic data, where matching filters are convolutional filters that minimize the sum-squared error between two signals. Since in the Fourier domain, a matching filter is the spectral ratio of the two signals, we extend the well known surface-consistent hypothesis such that the data term is a trace-by-trace spectral ratio of two data sets instead of only one (i.e. surface-consistent deconvolution). To avoid unstable division of spectra, we compute the spectral ratios in the time domain by first designing trace-sequential, least-squares matching filters, then Fourier transforming them. A subsequent least-squares solution then factors the trace-sequential matching filters into four operators : two surface-consistent (source and receiver), and two subsurface-consistent (offset and midpoint).

We present a time-lapse synthetic data set with nonrepeatable acquisition parameters, complex near surface geology, and a variable subsurface reservoir layer. We compute the four-operator surface-consistent matching filters from two surveys, baseline and monitor, then apply these matching filters to the monitor survey to match it to the baseline survey over a temporal window where changes are not expected. This algorithm significantly reduces the effect of most of the nonrepeatable parameters, such as differences in source strength, receiver coupling, wavelet bandwidth and phase, and static shifts. We compute the NRMS (normalized root mean square difference) on raw stacked data (baseline and monitor) and obtained a mean value of 70%. This value was significantly reduced after applying the four-component surface-consistent matching filters to about 15%.

INTRODUCTION

It has become an industry practice to acquire multiple seismic surveys at regular time intervals to monitor subsurface changes due to hydrocarbon production or fluid injection. Many of the early published case studies of monitoring the subsurface (Greaves and Fulp, 1987; Wang and Nur, 1989; Johnstad et al., 1993) allowed researchers to see the potential of this technology. As exploration seismologists, our main objective is to obtain an image that represents the "true" subsurface change. This goal is always challenged by the fact that seismic acquisition and processing are nonrepeatable (Ross and Altan, 1997; Jack, 1998; Landrø, 1999; Rickett and Lumley, 2001). Differences caused by nonrepeatability issues can divert our attention from differences caused by rock property changes.

It is common to have unavoidable differences in acquisition geometry between repeated seismic surveys, differences in the source waveforms, differences in receiver responses or even differences not related to equipment, such as near surface conditions (wet versus dry near surface, tides, winds, etc.) (Beasley et al., 1997; Ross and Altan, 1997; Rennie et al., 1997; Porter-Hirsche and Hirsche, 1998). Other differences can arise from inconsistent processing of time-lapse data due to different processing software or personnel, advances

in processing technologies, etc. (Jack, 1998).

A known process that reduces time-lapse nonrepeatability, which we term 'repeatability noise', is cross-equalization (Ross et al., 1996), which is a poststack process of amplitude scaling, phase matching, and static correction designed over a temporal window where changes are not expected. Generally, this cross-equalization process reduces the nonrepeatablity effects in seismic acquisition and processing and produces a better time-lapse image (Ross et al., 1996; Rickett and Lumley, 2001). Other time-lapse processing techniques are prestack "parallel" processing and "simultaneous" processing described by Lumley et al. (2003) that aim to reduce undesired time-lapse differences without match filtering. These are step-by-step time-lapse processing flows available in commercial software and all of them, poststack and prestack, are collectively called cross-equalization (XEQ) (Lumley et al., 2003).

The minimization of repeatability noise can be difficult, particularly if it occurs late in the processing flow. Instead, we propose a method that analyzes and equalizes much of the repeatability noise at the very beginning of the processing workflow. This method combines two basic concepts that are widely used in geophysical data processing: surface-consistency and matching filters.

The surface-consistent model was first introduced by Taner and Koehler (1981) who suggested the recorded seismic trace can be modeled as the convolution of each trace's source effect, receiver effect, offset effect and common midpoint (CMP) effect. This model is similar to the one used for solving the statics problem by Taner et al. (1974) and Wiggins et al. (1976). The surface-consistent model has been used in many studies to obtain a more accurate and stable deconvolution (Morley and Claerbout, 1983; Levin, 1989; Cambois and Stoffa, 1992; Cary and Lorentz, 1993), amplitude adjustment (Yu, 1985), and phase-rotation (Taner et al., 1991). Most of these algorithms are used routinely in seismic data processing sequences including those applied to data collected for monitoring studies.

The second well-known concept utilized in this paper is the shaping or matching filter (Claerbout, 1976, p.130-133; Robinson and Treitel, 1980, ch.1, 8, and 14). This is a filter designed to alter the shape of an input signal in order to obtain a desired output signal. In other words, it is a convolutional filter that minimizes the sum-squared difference between two signals. Matching filters are often computed as trace-by-trace operators to correct for time shift, amplitude variation, and phase and bandwidth in a surface-consistent manner or as global filters from baseline and monitor surveys (Ross et al., 1996).

In this paper we discuss the surface-consistent hypothesis and the theory of matching filters. Then we show how to extend the surface-consistent model to include more than one data set. We also discuss the relationship between spectral ratios and matching filters. Finally, we present an analysis of a modeled time-lapse synthetic data set that has many of the complexities generally observed in a real data set.

THEORY

In this section, we review the surface-consistent hypothesis and associated assumptions. Then we extend the model to represent two data sets instead of only one as in, for example,

surface-consistent deconvolution. Finally we formulate the theory of surface-consistent matching filters.

Surface-consistent hypothesis

Sheriff (1975) reviewed the factors affecting the seismic data amplitudes, and Taner and Koehler (1981) considered the effects of the same factors on the seismic spectra. Conceptually, the earth is considered to be separable into a thin near surface layer, subject to weathering effects and other seasonal changes, and the deeper subsurface where such changes are largely absent. The near surface layer can be considered to be a filter that modulates a wave traveling through it. Subsurface effects are more likely to be nonstationary but can be also approximated by a filter in a suitably restricted time zone.

Taner and Koehler (1981) proposed the surface-consistent model for a trace that has been gained, and has initial, approximate corrections for moveout and statics. Conceptually, the model separates near surface effects from subsurface effects through the dependence of the data upon the acquisition coordinates. Variations in the data that depend strongly on the source or receiver coordinates are assumed to arise from features in the very near surface. Alternatively, data variations that depend more strongly on midpoint and offset coordinates are attributed to features in the deeper subsurface. Taner and Koehler (1981) model represented the trace as the convolution of four terms expressed by:

$$d_{ij}(t) \approx \underbrace{s_i(t) * r_j(t)}_{Near-surface} * \underbrace{h_k(t) * y_l(t)}_{Subsurface}, \tag{1}$$

where " $*$ " denotes convolution in the time domain, t, and

- $d_{ij}(t)$: Seismic trace resulting from the ith source recorded into the jth receiver.

- $s_i(t)$: Source response at surface location i. This term includes such things as the source strength and waveform, and any attenuation or ghosting near the source location.

- $r_j(t)$: Receiver response at surface location j. This term contains the receiver coupling strength and the influence of geology near the receiver on the recorded waveform.

- $h_k(t)$: Offset response at offset location k. This contains subsurface effects that are offset dependent such as spherical divergence, or residual moveout, or surface waves, or AVO.

- $y_l(t)$: Midpoint term modeling the subsurface response below surface location l. Usually considered to be proportional to normal-incidence reflectivity, this contains the response of all traces with common midpoint and may include multiples and attenuation along the raypath.

In equation 1, the first two terms are source consistent and receiver consistent and describe effects attributable to the near surface. The second two terms are offset consistent and

midpoint consistent and describe effects attributable to the subsurface. In this paper, we use the term "four-component surface-consistent" to exactly mean the previous distinction. We assume a 2D acquisition geometry where receiver positions are evenly spaced and define a regular grid such that index j denotes a single grid cell. We also assume that the shot locations fall on this regular grid and that shot index i denotes the grid location of a given shot. Offset location k can now be computed as $k = |i - j|$, as well as midpoint location, l, where $l = \frac{1}{2}(i + j)$ (Technically midpoint locations define a regular grid with half the spacing of the receiver grid).

Equation 1 is a trace model and is not "derived" from any wave-theoretical concepts. Consequently, even the best noise-free data will never be described exactly by this equation. For example, the surface-consistent model is manifestly stationary (convolution is a stationary operation) and nonstationary effects such as moveout and anelastic attenuation can only be modeled approximately by restricting the analysis to small time windows. The introduction of the offset term and the midpoint term by Taner and Coburn (1980) and Taner and Koehler (1981) improved the fit to the data. Artifacts due to stretching and muting are assumed to be in offset terms (Taner and Koehler, 1981). Midpoint terms are assumed to be the normal incidence reflectivity where all traces at the same midpoint location contain the same subsurface information (Taner and Koehler, 1981). This normal incidence process is well approximated by applying corrections such as field statics (land data), spherical divergence, and normal moveout (Taner and Koehler, 1981; Claerbout, 1986; Cambois and Stoffa, 1992). In summary, equation 1 is an approximate trace model with a long history of successful applications. As in previous work, we use equation 1 to develop an overdetermined system of linear equations whose solution gives the four surface-consistent terms.

Extending the surface-consistent hypothesis to time-lapse data

We extend the surface-consistent data model to the case of designing matching filters to equalize two seismic surveys. Any trace in a baseline seismic survey may be modeled as follows:

$$d_1(t) \approx s_1(t) * r_1(t) * h_1(t) * y_1(t), \tag{2}$$

where we have suppressed the subscripts i, j, k, and l that denote explicit surface locations and simply use the subscript 1 to refer to the baseline survey. Similarly, the corresponding trace from a monitor seismic survey (with subscript 2) may be modeled as

$$d_2(t) \approx s_2(t) * r_2(t) * h_2(t) * y_2(t). \tag{3}$$

Here we implicitly assume that the two surveys have exactly the same geometry. Fourier transforming equations 2 and 3, forming their ratio, and linearizing by taking the logarithm of both sides, we obtain

$$\log\left(\frac{\widehat{d}_1(\omega)}{\widehat{d}_2(\omega)}\right) \approx \log\left(\frac{\widehat{s}_1(\omega)}{\widehat{s}_2(\omega)}\right) + \log\left(\frac{\widehat{r}_1(\omega)}{\widehat{r}_2(\omega)}\right) + \log\left(\frac{\widehat{h}_1(\omega)}{\widehat{h}_2(\omega)}\right) + \log\left(\frac{\widehat{y}_1(\omega)}{\widehat{y}_2(\omega)}\right), \tag{4}$$

where ω is frequency, the "$\widehat{}$" denotes the Fourier transform. The left-hand side of equation 4 is the data log spectral ratio and the right-hand side contains the sum of surface-consistent terms. Using equation 4 to form a linear system of equations, we can create a separate linear

system for each frequency, where each such system has one equation per trace. Provided that the number of traces exceeds the number of shots plus the number of receivers plus the number of offsets plus the number of midpoints, equation 4 can be used to build an overdetermined system of linear equations whose least-squares solution estimates the desired surface-consistent terms. In the next section, we will show that the Fourier transform of a matching filter is a spectral ratio. Hence, the spectral ratios in equation 4 define a set of four-component surface-consistent matching filters.

Matching filters and spectral ratios

A matching filter, also called a shaping filter, (Claerbout, 1976, p.130-133; Robinson and Treitel, 1980, ch.1, 8, and 14) is a convolutional filter that minimizes the sum-squared difference between two signals. The formulation of this is

$$m(t) * d_2(t) = d_1(t), \tag{5}$$

and the least squares solutions is obtained by minimizing

$$\sum_t \left(m(t) * d_2(t) - d_1(t) \right)^2 = \min, \tag{6}$$

where $m(t)$ is the time-domain matching filter which minimizes differences between two signals, d_1 and d_2. In the frequency domain, equation 5 can be solved exactly as:

$$\widehat{m}(\omega) = \frac{\widehat{d_1}(\omega)}{\widehat{d_2}(\omega)}. \tag{7}$$

Equation 7 is exact, but the spectral division renders it unstable if the data are band-limited or if noise dominates. Thus we see that a spectral ratio is the frequency domain expression of the matching filter, and so the various ratio terms in equation 4 are actually matching filters. We suggest a stable alternative to the spectral ratio by solving the time-domain least squares problem in equation 6, then transforming the solution to the frequency domain to obtain a stable spectral-ratio estimate.

Now that we have shown that a matching filter in the time domain is equivalent to a spectral ratio in frequency domain, we can elaborate more on equation 4. The left-hand side of equation 4 is a trace-by-trace matching filter computed in the time domain by least squares and then transformed to the frequency domain. The surface-consistent system is solved independently for each frequency (Figure 1), followed by inverse Fourier transform of the solution back to time domain. The result is a set of surface-consistent convolutional filters that will match survey 2, monitor, to survey 1, baseline, in the least squares sense.

SPECTRAL DECOMPOSITION

After solving the time-domain least-squares matching filter in equation 5 for each pair of traces in the two surveys and transforming the result to the frequency domain, we now consider a second least-squares decomposition of the solution into its four-component surface-consistent terms. This can be formulated as a general linear inverse problem (Wiggins et al., 1976) such that

$$\mathbf{G}\mathbf{m}(\omega) = \mathbf{d}(\omega) \tag{8}$$

where $\mathbf{G}$ represents the seismic geometry matrix (Figure 2), and $\mathbf{m}$ is a vector of surface-consistent terms (the unknowns). Usually the number of columns of $\mathbf{G}$ equals the total number of sources (N_s) + total number of unique receivers (N_r) + total number of offset bins (N_h) + total number of midpoint bins (N_y). Similarly, the number of rows of $\mathbf{G}$ equals the total number of traces ($N_t = N_s N_r$, assuming each shot to have the same number of receivers), which is equal to the length of $\mathbf{d}$. The number of columns of $\mathbf{G}$ can be reduced by solving for only selected midpoints and offsets and interpolating between solution points. In this paper, we solve for all midpoints and offsets.

For all but the most trivial geometries, the problem is overdetermined (more equations, N_t, than unknowns, $N_s + N_r + N_h + N_y$). This is similar to the classic residual statics estimation problem (Wiggins et al., 1976). The problem is also known to be underconstrained (deficient in the number of independent equations available to solve for the unknowns). Wiggins et al. (1976) showed that the residual statics problem, which is essentially similar to this one, does not constrain "long wavelength" solutions. Mathematically, this is because $\mathbf{G}^T\mathbf{G}$ has a non-trivial null space, or equivalently, $\mathbf{G}$ has some zero singular values (Aster et al., 2005).

If $\mathbf{m}^\dagger$ represents a vector of the four unknowns, then the result of the least-squares decomposition is:

$$\mathbf{m}^\dagger = (\mathbf{G}^T\mathbf{G} + \alpha^2\mathbf{I})^{-1}\mathbf{G}^T\mathbf{d}, \qquad (9)$$

where α is a regularization parameter (a small positive number that can be estimated using the L-curve method) (Aster et al., 2005), and $\mathbf{I}$ is the identity matrix. Note that the matrix $\mathbf{G}^T\mathbf{G} + \alpha^2\mathbf{I}$ is nonsingular since $\alpha^2\mathbf{I}$ was chosen to constrain the null space of $\mathbf{G}$. This method works well for a small data set like our example. However, with large data sets direct inversion of the system in equation 9 will be expensive, and usually iterative methods such as conjugate gradient or Gauss-Seidel are utilized (Morley and Claerbout, 1983; Wiggins et al., 1976; Cary and Lorentz, 1993)

TIME-LAPSE MODEL EXPERIMENT

For this experiment, we constructed a simple $2.5km$ wide and $1km$ thick $2D$ model. The model consists of five layers including a reservoir unit, $500m$ wide and $20m$ thick , between layers three and four. The velocity is homogeneous in each layer, except for the near surface layer, where random lateral variations were introduced. Using this geometry, we generated two earth models, a baseline model and a monitoring model (Figures 3(a) and 3(b)), with different near surface and reservoir velocities (Figures 3(c) and 3(d)). Velocity variation in the near surface due to seasonal soil variations is one of the nonrepeatability issues for land time-lapse data. In Canada, such seasonal variations can be extreme between winter and summer, and can also involve variations in near surface attenuation. Our baseline model had a slower near surface simulating summer acquisition while our monitor model had faster velocities simulating winter acquisition. We also included a variable Q (Figure 4(a)) in the near surface layer, which effectively means that the source wavelet shows variable bandwidth laterally along the line.

An acoustic finite-difference modeling algorithm was used to acquire 51 shot records at $50m$ shot interval using a receiver array of 101 geophones at $10m$ spacing. We used the

2D split-spread acquisition geometry and shot through the tail spread on each end. The maximum record length is $1s$ with a $4ms$ sampling interval. Each shot record and each receiver were scaled by randomly generated scalars (Figures 4(b) and 4(c)) to simulate variations in source strength and receiver coupling.

Raw shot records from the baseline and the monitor surveys are illustrated in Figures 5(a) and 5(b), respectively. There is a large difference between these two unprocessed shot records, Figure 5(c), particularly in arrival time of events, amplitude and phase. A commonly used metric that measures the similarities between traces is called NRMS (normalized root mean square difference) (Kragh and Christie, 2002). We computed the NRMS inside a window of approximately $300ms$ just above the reservoir unit ($\sim 0.75s$ in the middle of the shot record indicated by two dashed lines), and the result is shown in Figure 5(d) with a mean of 144.7%. NRMS is computed using the following relationship discussed in Kragh and Christie (2002):

$$NRMS(\%) = 200\frac{rms(base - monitor)}{rms(base) + rms(monitor)}. \tag{10}$$

Theoretical NRMS values range from 0 to 200% (Kragh and Christie, 2002), where low values correspond to similar traces, and high values correspond to extremely dissimilar ones. One possible way to reduce the difference observed in Figure 5(c) is by adding a constant time shift to the monitor shot record. Figure 6(a) is the same baseline shot record shown earlier, and Figure 6(b) is the same monitor shot record shown in Figure 5(b) shifted down by $26ms$ so that the middle reflector matches the same reflector on the baseline shot. Figures 6(c) and 6(d) illustrate their differences and their computed NRMS, respectively. Although the mean NRMS is reduced to 44.7% due to the added constant time shift, each monitor survey shot record requires a different time shift. Additionally, significant difference remains due to the mismatch in amplitude and phase.

Examining NRMS versus time shift of two noise-free signals (Figure 7(a)) shows a clear linear relationship (or $NRMS(\%) \approx 100(2\pi f\delta t)$, where f is the dominant frequency and δt is the time shift between the two traces) (Calvert, 2005). NRMS error versus amplitude difference (Figure 7(b)) is only linear for a small amplitude residual (or $NRMS(\%) \approx 100(\delta a)$, where δa is amplitude residual between the two traces) (Calvert, 2005). The high NRMS values, ranging from 120% to 150% seen in Figure 5(d), suggest a highly nonrepeatable time-lapse experiment, as we had intended our synthetic to be.

Computing surface-consistent matching filters

We have computed the four-component surface-consistent trace-by-trace matching filters inside a $300ms$ window above the target (Figures 5(a) and 5(b)) for all 51 shot records. Using equation 9, we decomposed these trace-by-trace matching filters into a set of surface-consistent matching filters. There are similarities between the interpretation of the surface-consistent log spectral decomposition of the matching filters and that of the residual statics described by Wiggins et al. (1976). In the residual statics problem, contribution from the source and receiver terms as well as structure and residual normal moveout (NMO) were clear and reported by Taner et al. (1974). Similar distinctions were observed in the surface-consistent matching filters where each of the four terms collects different effects.

The source and receiver terms

Since we are decomposing a log spectral ratio of two data sets, we interpret the source term as a log spectral ratio of the two corresponding source signatures, which we take to include the actual source wavelets and local modifications caused by source strength variations and attenuation. After exponentiation and inverse Fourier transform, this yields a set of time-domain filters that match each source record in the monitor survey to the baseline survey. Similarly, the receiver term is a log spectral ratio of the two corresponding receivers' response and the near surface effects around each receiver. When exponentiated and inverse Fourier transformed, a set of time-domain filters is obtained that matches each receiver in the monitor survey to the baseline survey.

Figures 8(a) and 8(c) show the source and receiver components computed from the raw shot records of the baseline and the monitor surveys. In the source components, we notice variations in Figure 8(a) that correlate with changes seen in Figure 4(b) due to source strength variations between the two surveys, i.e around shot number 10, 25 and 40. Figure 8(b) illustrates the similarities between the mean shot filters, which we will refer to as source strength, and the ratio of baseline survey to monitor survey source strengths. Similar effects can also be seen in the receiver components in Figure 8(c) where variations in receiver couplings are known (Figure 4c). Figure 8(d) shows the similarities between the mean receiver filters, which we will refer to as receiver strength, and the ratio of baseline survey to monitor survey receiver strengths. Separation of the source signature or the receiver impulse response from the surrounding near surface geology effects is unnecessary, since we are primarily interested in applying these surface-consistent matching filters to the monitor survey (the survey in the denominator of equation 4) to reduce its mismatch with the baseline survey.

The offset and midpoint terms

The two other components computed in the study are offset and midpoint terms. Figure 9(a) shows the log-amplitude spectrum of the offset term. Muting the first breaks was necessary due to their interference with inside the reflections analysis window that occurred at about offset $400m$. Similar large amplitude estimates have been reported in the offset components by Cary and Lorentz (1993) and were attributed to coherent noise such as ground roll. In this study, after we muted the first breaks (Figures 5(a) and 5(b)), the newly computed offset terms were lower in amplitude than previously computed offset terms and smoother than the source and receiver terms. A smoother offset term is attributed to the fact that there are more traces contributing to each offset than to the source and receiver terms (Cary and Lorentz, 1993). Figure 9(b) represents the average over frequency of the offset filters, referred to as offset strength, shown in Figure 9(a) where amplitude values are high before offset number 40 but reduce to unity beyond, due to absence of data.

The midpoint filters in Figure 9(c) show rapid variations compared to the other components. Similar observations have been reported by Cary and Lorentz (1993) for the surface-consistent deconvolution problem. The midpoint term collects more noise than any other term because of the low fold (low number of traces per midpoint), but that can be minimized if smoothing is applied. In this study, the overall strength of the midpoint filter

(Figure 9(d)) is small (averaging about one), hence we decided not to apply smoothing.

FILTER APPLICATION AND ANALYSIS

Applying the computed four-component surface-consistent matching filters in Figures 8(a), 8(c), 9(a), and 9(c) to the monitor survey, we obtain a new survey that more closely matches the baseline survey. Figure 10(b) illustrates a surface-consistent matched monitor survey that compares to the same shot record in the baseline survey (Figure 10(a)). The new difference is shown in Figure 10(c). Note that the mismatch observed in Figure 5 has been reduced significantly, and that the computed NRMS in the window of analysis (between the two dashed lines) has reduced to a mean of 26.8%.

In the next two sections, we will compare trace-by-trace and surface-consistent matching filters, before and after stack, and then examine the effects of the surface-consistent terms.

Trace-by-trace and Surface-consistent matching filters

The surface-consistent method separates the seismic trace into surface (source and receiver) and subsurface (offset and midpoint) components. Each of these four terms has a different signature that can be examined and compared. In other words, traces that share the same source will always have the same source filter, and similarly those traces recorded by the same receiver will always have the same receiver filter. For comparison, we show results from application of trace-by-trace matching filters that are used as input to our surface-consistent decomposition. The following two examples demonstrate this difference clearly. Figure 11(a) is the difference between a trace-by-trace matching filter applied to a single shot of the monitor survey and the baseline survey. In this example, the trace-by-trace matching filters reduced much of the mismatch between the two surveys and the mean NRMS is approximately 25%. It is slightly less than that obtained by the four-component surface-consistent matching filters shown in Figure 10(d). Figure 11(b) is the difference between the matched monitor survey stack and the baseline survey stack, for trace-by-trace matching filters. The mean NRMS computed in the filter window (between the two gray lines) in the figure is about 35%. Comparing this result to that obtained from applying the four-component surface-consistent matching filters (Figure 12(f)), the latter one is preferred due to its low NRMS error of 15.7%. In summary, on a single shot record trace-by-trace matching filters produce a slightly lower NRMS (25%) than surface-consistent matching filters (26.8%). However, when the data are stacked and NRMS are computed, the surface-consistent matching filters produce a much better result compared to the trace-by-trace matching filters (15.7% versus 35%). Stacking actually increases the NRMS for trace-by-trace matching filters while it decreases for surface-consistent matching filters.

The effects of the surface-consistent terms

Computing the four components (source, receiver, offset, and midpoint) but only applying two terms (source and receiver) is a common practice for residual statics solutions. However, because we are introducing a new surface-consistent method, we want to compare the results of applying two terms, three terms and all four terms. The results displayed

in Figures 12(a), 12(c), and 12(e) are difference plots for two, three, and four components, respectively, for a single shot. The two-component difference in the prestack example seems to have resolved some of the amplitude variation, time shifts, and phase. Its mean NRMS is 30% (Figure 12(a)), and similarly after stacking the gathers (Figure 12(b)), the residual remains relatively high with mean NRMS of about 32%. Since we are computing NRMS in the window just above the reservoir, source and receiver terms will not describe all the changes in this interval, as in the surface-consistent hypothesis, and much of the changes will be described by offset and midpoint components.

Application of three components (Figure 12(c)) results in some residual amplitude and a calculated mean NRMS of about 30%, while after stacking the gathers the difference decreased significantly, with mean NRMS of about 18.7% (Figure 12(d)). The four-component solution (Figure 10(c)) shows slight improvement over the three-component solution, and its mean NRMS is about 26%. Its stacked result in Figure 12(f) has the smallest residual of all, with a mean NRMS of about 15.7%.

Figure 13 illustrates the NRMS difference after different stages of processing for two different data sets. A published example of real data set from Gulf of Mexico by Helgerud et al. (2011) shows the NRMS is about 70% at the raw stack stage, and at final stack they reported an improvement to about 28%. In our modeled data set we started with NRMS of about 144.7% in the prestack stage, then about 70% in the raw stack (similar to the published example), then a significant improvement after the four-component surface-consistent matching filters; and after final stack the NRMS is about 15.7%. The matching filter technique used by Helgerud et al. (2011) is a post-stack process, and in contrast, we applied prestack four-component surface-consistent matching filters.

CONCLUSIONS

We have developed a method to design surface-consistent matching filters that can be used to match one data set to another in a time-lapse experiment. The new algorithm is similar to the well known surface-consistent deconvolution except that the data required are the trace-by-trace spectral ratios of two data sets instead of the spectrum of a single one. We have demonstrated that computing the spectral ratios in a stable manner is possible by Fourier transforming the trace-sequential least-squares matching filters. A subsequent least-squares solution then factors the trace-sequential matching filters into four surface-consistent operators: source, receiver, offset, and midpoint.

Using a synthetic seismic model, we applied the four-term surface-consistent matching filters to the monitor survey to match it to the baseline survey over a temporal window where changes were not expected. The prestack nonrepeatable difference between the matched monitor survey and the baseline survey was quite small compared to the difference before applying the matching filters. The simulated nonrepeatable effects include reflection amplitude variations, wavelet bandwidth and phase differences, and static shifts. We have demonstrated that on single trace gathers, trace-sequential matching filters could reduce the differences between time-lapse surveys when compared to surface-consistent matching filters. However, after stacking the trace-sequential matching exhibits high NRMS (35%) while the surface-consistent matching filters improve signifi-

cantly (NRMS of 15.7%). We have also shown that applying the four-component surface-consistent matching filters yielded the lowest NRMS difference (15.7%) compared to applying only two-term or even three-term surface-consistent matching filters.

ACKNOWLEDGMENTS

REFERENCES

Aster, R. C., Borchers, B., and Thurber, C. H. (2005). *Parameter estimation and inverse problem*.

Beasley, C. J., Chambers, R. E., Workman, R. L., Craft, K. L., and Meister, L. J. (1997). Repeatability of 3-d ocean-bottom cable seismic surveys. *TLE*, (16):1281–1285.

Calvert, R. (2005). Insights and methods for 4d reservoir monitoring and characterization. *SEG/EAGE DISC course*.

Cambois, G. and Stoffa, P. L. (1992). Surface-consistent deconvolution in the log/fourier domain. *Geophysics*, (57):823–840.

Cary, P. W. and Lorentz, G. A. (1993). Four-component surface consistent deconvolution. *Geophysics*, (58):383–392.

Claerbout, J. F. (1976). *Fundamentals of Geophysical Data Processing With Applications to Petroleum Prospecting*.

Claerbout, J. F. (1986). Simultaneous pre-normal and post-normal moveout deconvolution. *Geophysics*, (51):1341–1354.

Greaves, R. J. and Fulp, T. J. (1987). Three-dimensional seismic monitoring of an enhanced oil recovery process. *Geophysics*, (52):1175–1187.

Helgerud, M. B., Miller, A. C., Johnston, D. H., Udoh, M. S., Harris, C., Jardine, B. G., and Aubuchon, N. (2011). 4d in the deepwater gulf of mexico: Hoover, madison, and marshall fields. *TLE*, (30):986–1079.

Jack, I. (1998). Time-lapse seismic in reservoir management. *SEG short course notes*.

Johnstad, S. E., Uden, R. C., and Dunlop, K. N. B. (1993). Seismic reservoir monitoring over the oseberg field. *FB*, (11):177–185.

Kragh, E. and Christie, P. (2002). Seismic repeatability, normalized rms, and predictability. *TLE*, (21):640–647.

Landrø, M. (1999). Repeatability issues of 3-d vsp data. *Geophysics*, (64):1673–1679.

Levin, S. A. (1989). Surface-consistent deconvolution. *Geophysics*, (54):1123–1133.

Lumley, D., Adams, D. C., Meadows, M., Cole, S., and Wright, R. (2003). 4d seismic data processing issues and examples. *SEG Exp. Abst.*, (22):1394–1397.

Morley, L. and Claerbout, J. (1983). Predictive deconvolution in shot-receiver space. *Geophysics*, (48):515–531.

Porter-Hirsche, J. L. and Hirsche, K. W. (1998). Repeatability study of land data acquisition and processing for time lapse seismic. *SEG Exp. Abst.*

Rennie, J., Alexandre, R., and Ronen, S. (1997). Sensitivity of repeated 3-d seismic surveys to geometry variations - a controled experiment. *SEG Exp. Abst.*

Rickett, J. E. and Lumley, D. E. (2001). Cross-equalization data processing for time-lapse seismic reservoir monitoring: A case study from the gulf of mexico. *Geophysics*, (66):1015–1025.

Robinson, E. A. and Treitel, S. (1980). Geophysical signal analysis. *Prentice-Hall, Inc.*

Ross, C. P. and Altan, M. S. (1997). Time-lapse seismic monitoring: Some shortcomings in nonuniform processing. *TLE*, (16):931–937.

Ross, C. P., Cunningham, G. B., and Weber, D. P. (1996). Inside the crossequalization black box. *TLE*, (15):1233–1240.

Sheriff, R. E. (1975). Factors affecting amplitudes. *Geoph. Prosp.*, (23):125–138.

Taner, M. T. and Coburn, K. W. (1980). Surface consistent estimation of source and receiver response functions. *50th Annual International SEG Meeting*.

Taner, M. T. and Koehler, F. (1981). Surface consistent corrections. *Geophysics*, (46):17–22.

Taner, M. T., Koehler, F., and Alhilali, K. A. (1974). Estimation and correction of near-surface time anomalies. *Geophysics*, (39):441–463.

Taner, M. T., Lee, L., and Baysal, E. (1991). Static corrections: time, amplitude, and phase. *SEG Exp. Abst.*

Wang, Z. and Nur, A. (1989). Effect of temperature on wave velocities in sandstones and sands with heavy hydrocarbons, *in* nur, a. and wang, z., eds., seismic and acoustic velocities in reservoir rocks. *Soc. Expl. Geophysics*.

Wiggins, R. A., Larner, K. L., and Wisecup, R. D. (1976). Residual static analysis as a general linear inverse problem. *Geophysics*, (41):922–938.

Yu, G. (1985). Offset-amplitude variation and controlled-amplitude processing. *Geophysics*, (50):2697–2708.
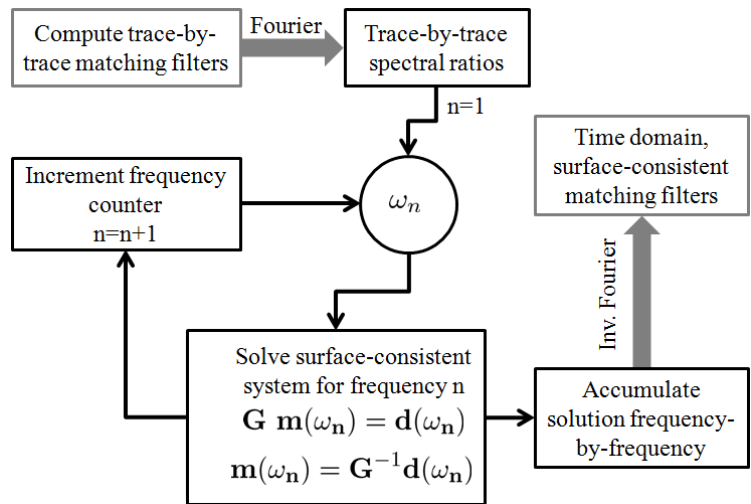
FIG. 1: Processing workflow for the trace-by-trace surface-consistent matching filters.
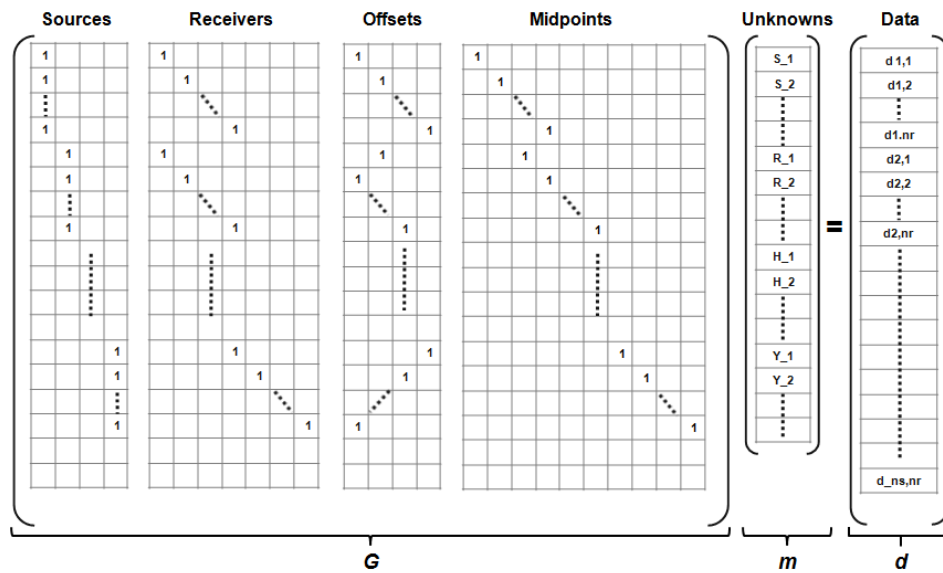
FIG. 2: Matrix structure of the system of linear equation described in equation 8; the number of columns of $\mathbf{G}$ = number of sources + number of unique receivers + number of unique offsets + number of midpoints and the number of rows of $\mathbf{G}$ = total number of traces; the length of $\mathbf{d}$ = total number of traces.
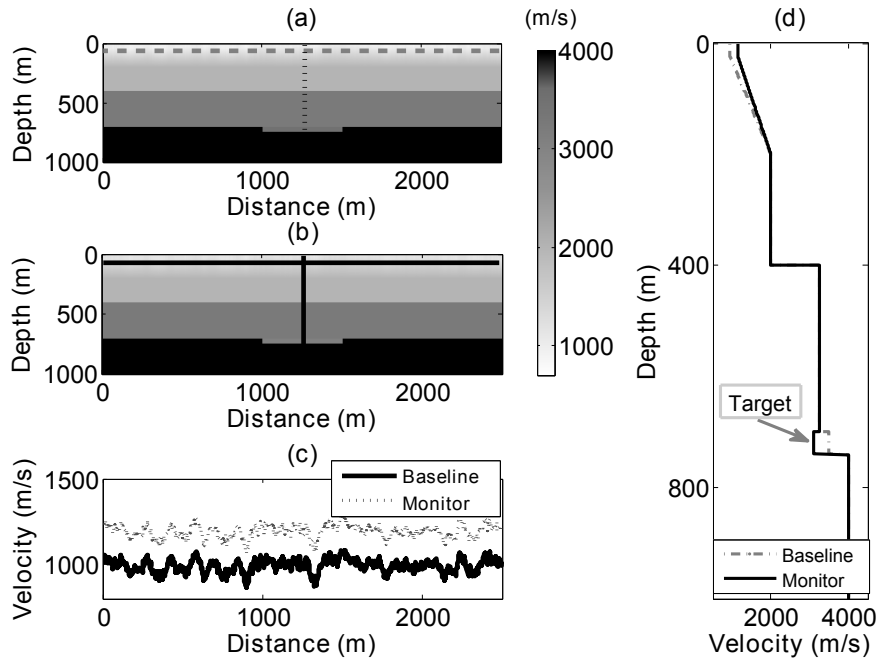
FIG. 3: Two earth models representing a baseline survey and a monitor survey (a) where the difference is in the near surface velocity (b) (showing effects of dry vs wet climate) and in the reservoir unit as shown in (c) (showing effects of fluid production).
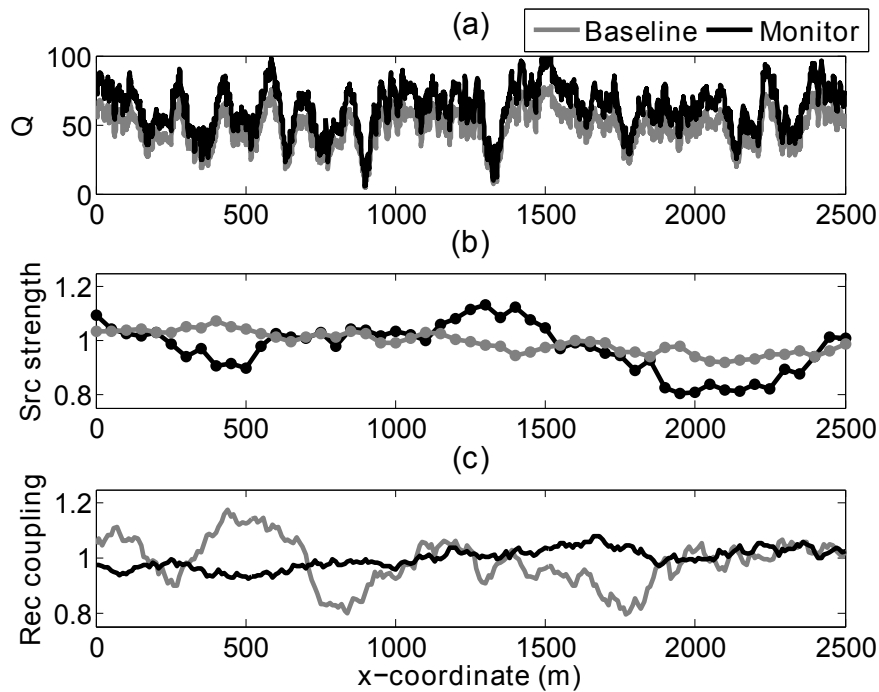
FIG. 4: Horizontal profile of near surface attenuation for baseline model (gray line) and monitor model (black line)(a), source strength (b), and receiver coupling (c).
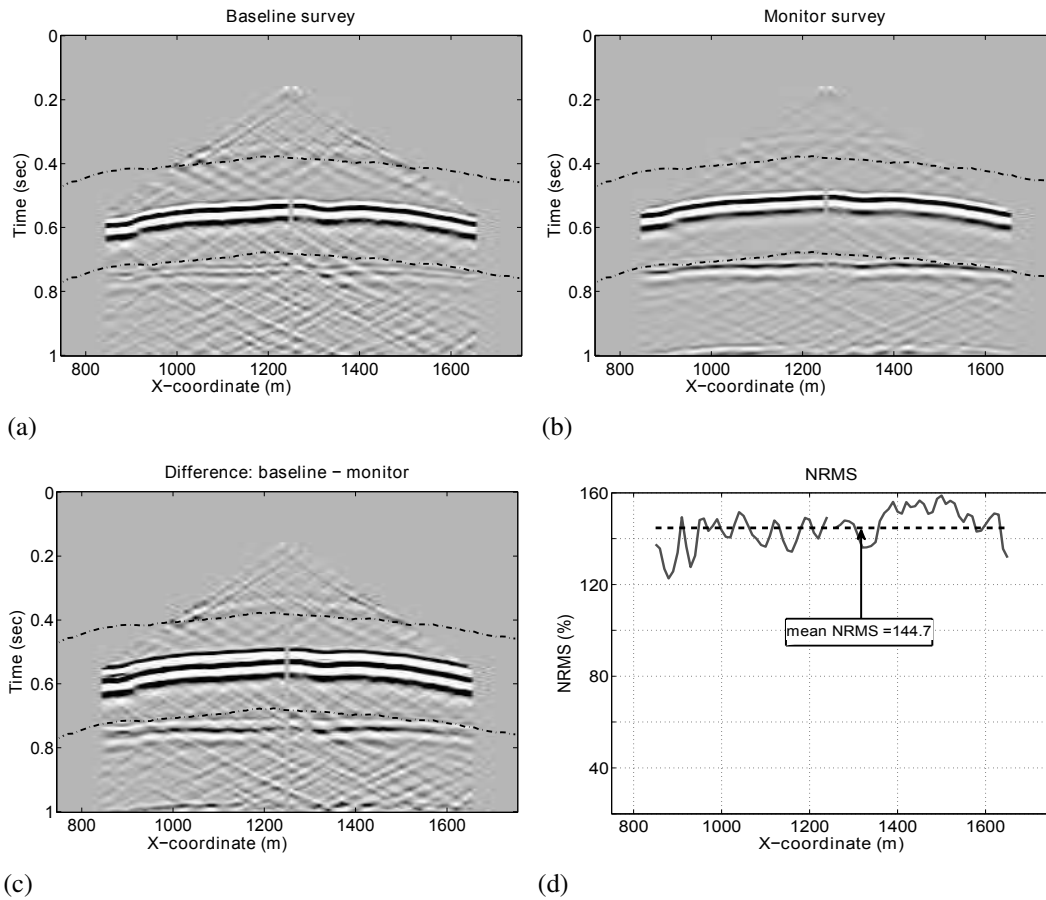
FIG. 5: Two shot records, source location at $1250m$, from the baseline survey (a) and the monitor survey (b). (c) shows the difference between (a) and (b), and (d) shows the NRMS computed between the two dotted lines (the analysis window) of the difference plot. Note the mean NRMS is 144.7% which means both surveys are highly dissimilar.
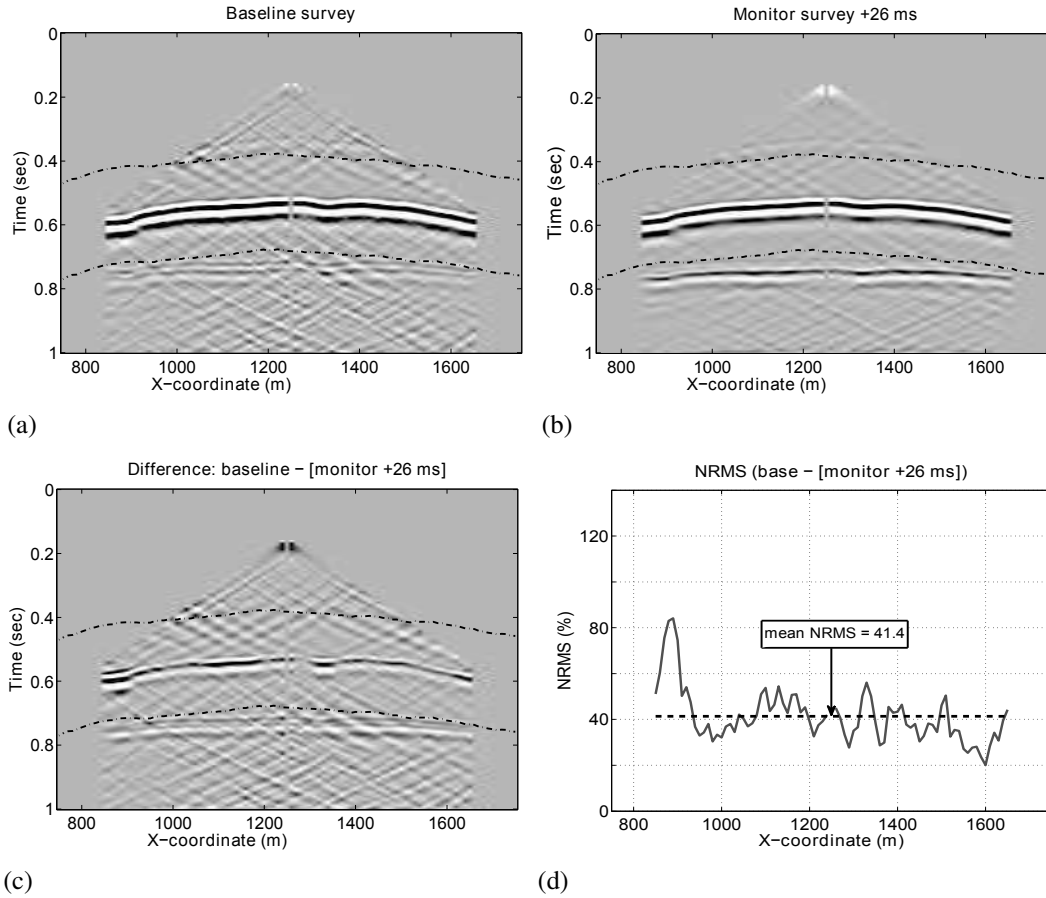
FIG. 6: Baseline shot (a), similar to Figure **??**, and monitor shot with $+26ms$ time shift (b). The difference of (a) and (b) is shown is (c), and (d) shows the NRMS computed between the two dotted lines (the analysis window) of the difference plot. Note that the mean NRMS has decreased to 41.4% but there is a significant amplitude difference.
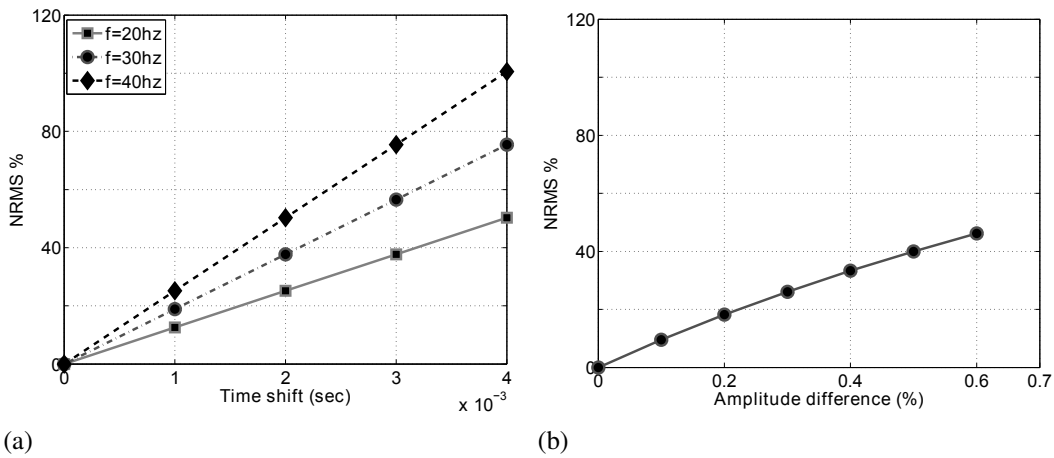
FIG. 7: NRMS sensitivity tests where (a) is NRMS versus time shift for three dominant frequencies and (b) is NRMS versus amplitude difference between two noise free traces.

(a)

(b)

(c)

(d)
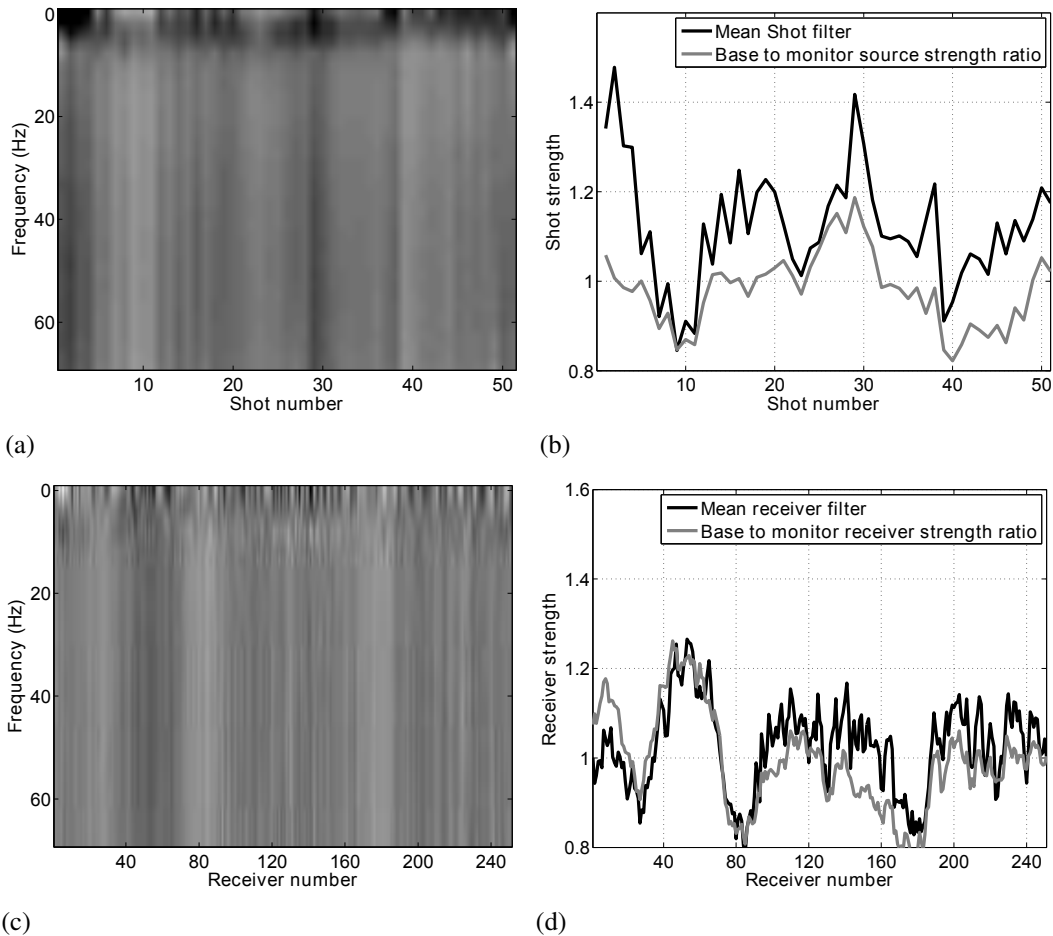
FIG. 8: In (a) is the log amplitude spectra of the source filters computed using equation 9. In (b) is a comparison of the average over frequency of the shot filters, referred to as source filters strength, in black line versus the ratio of the baseline survey source strength to the monitor survey source strength in gray line. The log amplitude spectra of the receiver components is shown in (c) and in (d) is a comparison of the receiver filter strength (black line) versus the receiver strength ratio of both surveys (light gray line).
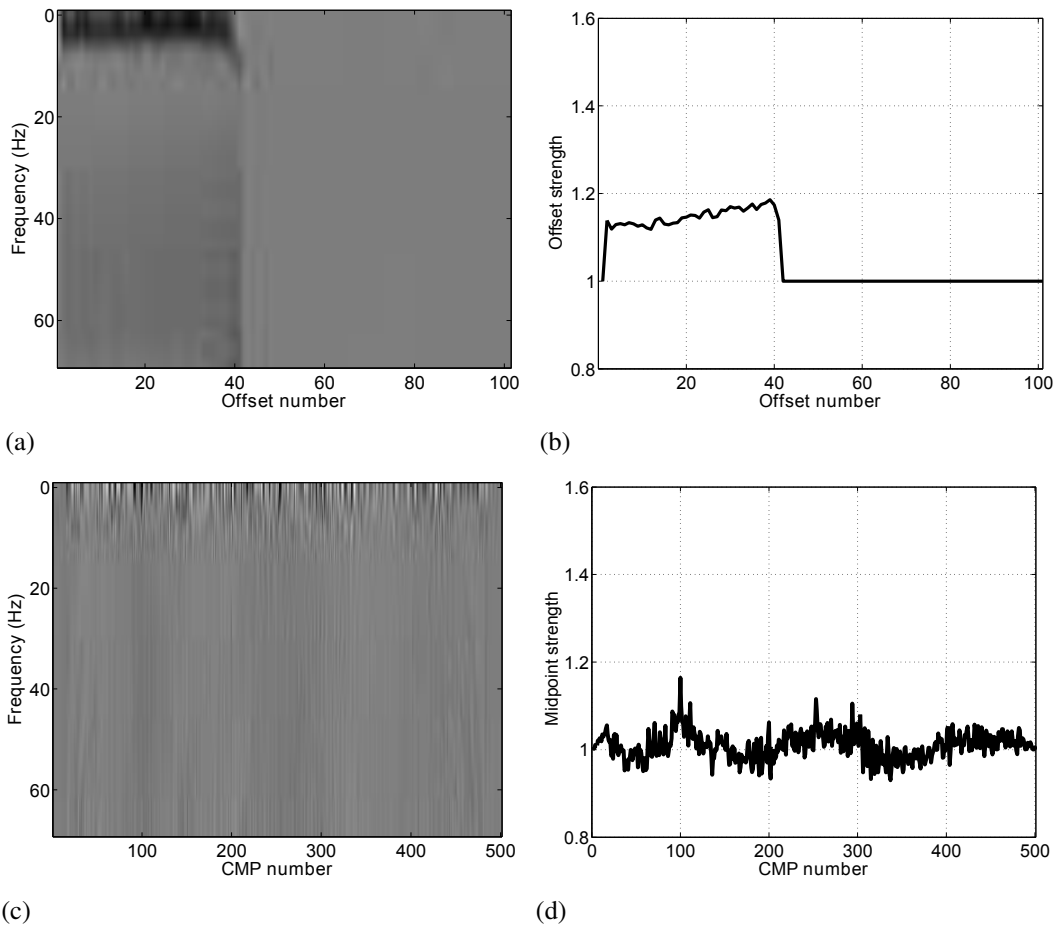
FIG. 9: In (a) is the log amplitude spectra of the offset filters and in (b) is the offset filter strengths computed as the average over frequency. Similarly, in (c) is the log amplitude spectra of the midpoint filters and in (b) is the midpoint filter strengths computed as the average over frequency.

(a) (b)

(c) (d)
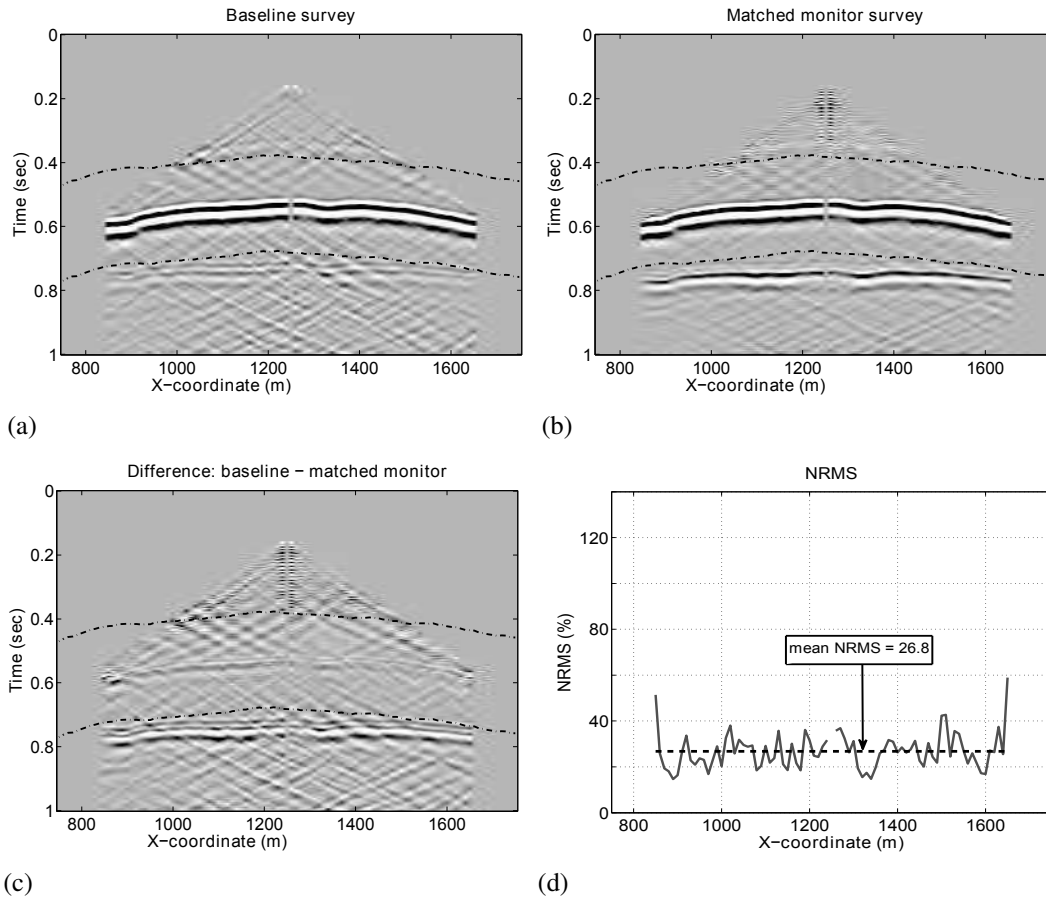
FIG. 10: Baseline shot shown in (a), the monitor shot after applying the four-component filters to it in (b) (hereafter we named it matched monitor survey). The difference is shown in (c) and the computed NRMS between the two dashed lines is shown in (d). Note that the mean NRMS is down to 26.8%.


(a) (b)
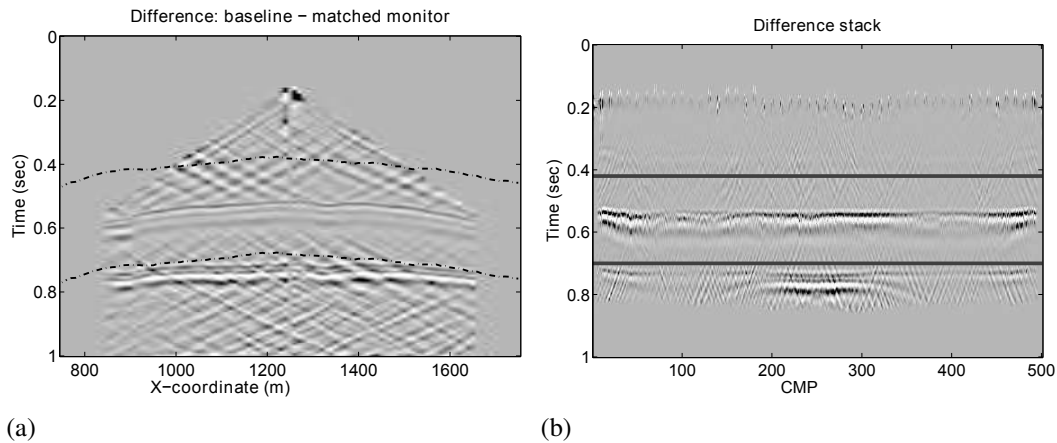
FIG. 11: In (a) is a difference plot between baseline shot and a trace-by-trace matched monitor shot (mean NRMS $\approx 25\%$). (b) stack of the difference between baseline and a trace-by-trace matched monitor (mean NRMS $\approx 35\%$).
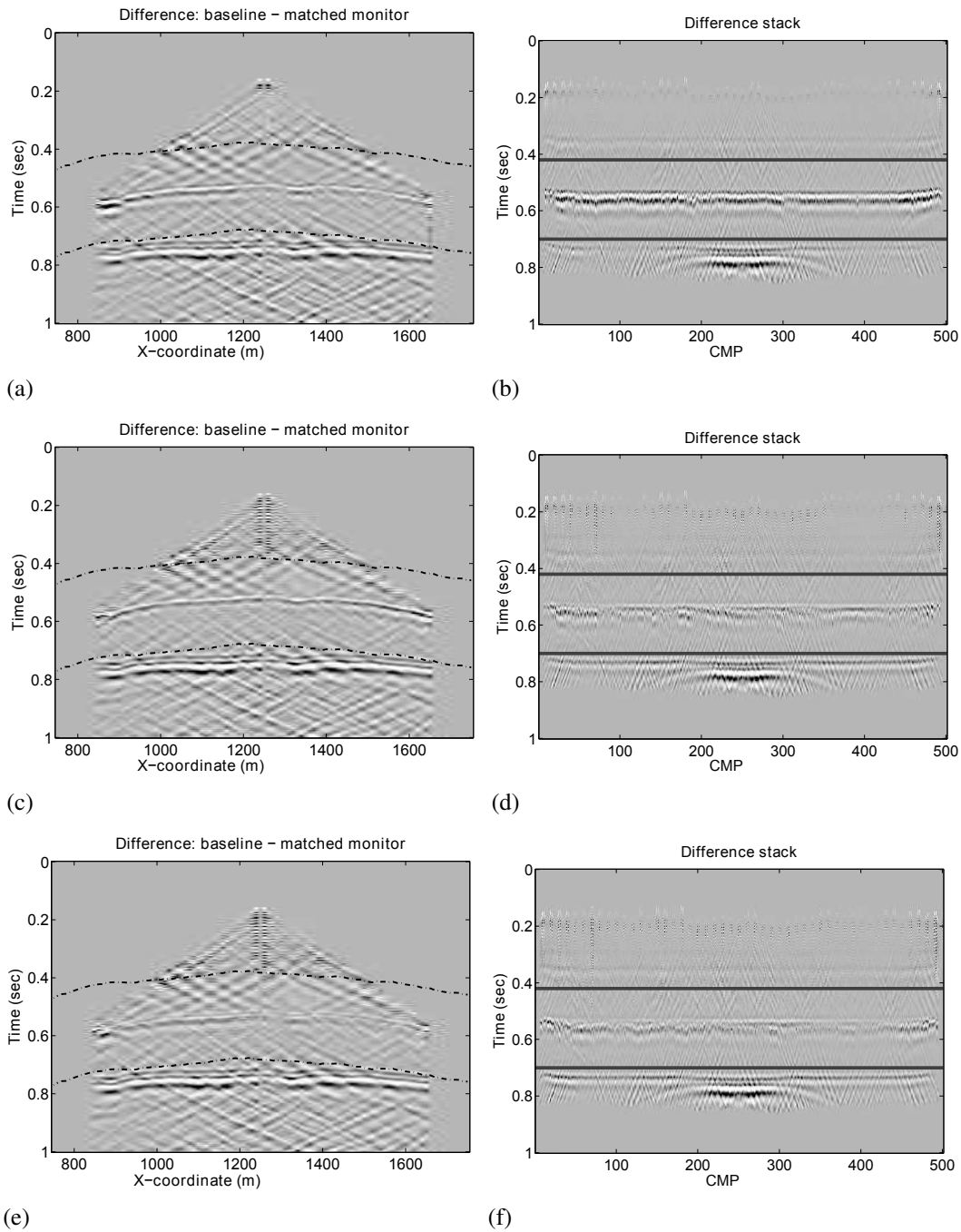
FIG. 12: a) is a prestack difference of the baseline and the matched monitor, with source and receiver terms applied, (mean NRMS $\approx 30\%$) and (b) shows the poststack difference (mean NRMS $\approx 32\%$). (c) is a prestack difference with three terms applied (source, receiver and offset) and the mean NRMS $\approx 28.5\%$ also in (d) is the poststack difference (mean NRMS $\approx 18.7\%$). (e) is a prestack difference plot with four-term filters applied (mean NRMS $\approx 26.8\%$) and (f) is the poststack difference (mean NRMS $\approx 15.7\%$).
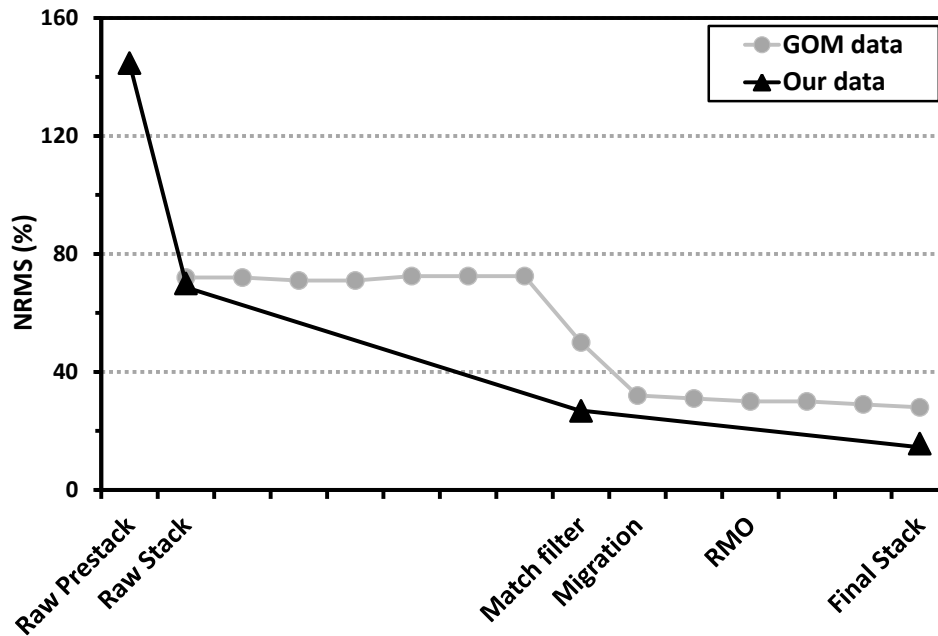
FIG. 13: NRMS difference after different stages of processing for two different data sets. The light gray line represent a published example of real data set from Gulf of Mexico by Helgerud et al. (2011) where at raw stack stage the NRMS is about 70% and at final stack they reported an improvement of about 28%. In our modeled data set we started with NRMS of about 144.7% in prestack stage, then about 70% at raw stack, then a significant improvement after the four-component surface-consistent matching filters and after final stack the NRMS is about 15.7%.